THIRTEENTH EUROPEAN ROTORCRAFT FORUM

2.14
Paper No. 59

COMPUTATION OF SUBSONIC AND TRANSONIC HELICOPTER ROTOR FLOW USING EULER EQUATIONS

E. Krämer, J. Hertel, S. Wagner

Universität der Bundeswehr München

Institut für Luftfahrttechnik und Leichtbau

September 8-11, 1987

ARLES, FRANCE

ASSOCIATION AERONAUTIQUE ET ASTRONAUTIQUE DE FRANCE

COMPUTATION OF SUBSONIC AND TRANSONIC HELICOPTER ROTOR FLOW USING EULER EQUATIONS

E. Krämer, J. Hertel, S. Wagner

Universität der Bundeswehr München

Institut für Luftfahrttechnik und Leichtbau

Abstract

A procedure for the computation of transonic steady and unsteady flow around helicopter rotors is presented.
The algorithm is based on the Euler equations and allows the computation of anisotropic rotational flow and thus an implicitly accurate calculation of shocks. In addition the capturing of the rotor wake and the tip vortex is provided for arbitrary tip shapes.
The code for the computation of steady, fully 3-D rotor flow is derived from the EUFLEX procedure originated by A. Eberle, that has successfully been applied to a lot of fixed wing configurations up to now. A finite-volume scheme based on the method of characteristic flux averaging solves the Euler equations formulated in the conservation form.
The discretization of the flow field is carried out in two different manners concerning the grid topology and the size of the physical domain. Calculations are presented for a non-lifting case and for a helicopter rotor in hover. The comparisons of the method in its present stage show good agreement with experimental data.

1. Introduction

For some years Euler methods have proved their efficiency in innumerable applications mostly to fixed wings or even to complete aircraft configurations.
Recently, several scientists are now engaged in applying the Euler equations to the complex case of rotational flow as it appears for instance in helicopter flight.
Before that, a lot of solution algorithms based on lifting surface, small pertubation or full potential theory have widely been used and still are, since they are much faster and require less storage than Euler methods. Nowadays as the computational capacities, both in storage and speed, have reached a higher level, the demands have increased, too.
The Euler equations, although more expensive, provide the advantages of being able to treat anisotropic and rotational flow and admit vortical solutions. This is essential for a correct prediction of transonic shocks and trailing vorticity, which are implicit parts of Euler solutions. Thus, unlike potential flow equations, Euler equations on principle allow the transport of vorticity, rollup of the wake following the blade, convection of the tip vortex past the blade and herewith consideration of blade vortex interactions, all of them being main characteristics of a helicopter rotor flowfield.

However, the applications of different Euler codes to this problem show,

that there are several limitations associated for example with the capturing of the tip vortex at smooth blade tips (Ref. 7), the geometry of the rotor wake or the convection of the tip vortex (Ref. 4-10). For this reason, more or less accurate wake models based on low order theory have to be coupled with the Euler codes in order to provide wake geometry, tip vortex location and induced velocities to be introduced into the solution process via effective angle of attack reduction (Ref. 7,9,10), velocity splitting (Ref. 6,4) and so on.
Reasons for these limitations are found within the numerical formulation of the Euler solvers. Especially the false diffusion of the tip vortex is due to artificial viscosity involved in some algorithms on one hand and to truncation errors on the other hand.

At least the first problem is alleviated by the use of the finite-volume EUFLEX code of A. Eberle (Ref. 1), which works without artificial viscosity terms and applies higher order differencing.
The problem of truncation errors will become less severe, if some substantial grid refinements were made in those regions, where the vortex path is presumed. This should be possible in view of the capacity of today´s supercomputers.

The present paper describes the initial stage of investigations, whether and to which degree of accuracy it is possible to predict all effects refering to the rotor wake without using any wake model.
Two parallel ways are persued, differing in the use of the body conforming grid around the blade. The first kind of discretization covers the whole rotor flow field, completely enclosing the rotor disk and the wake, which is contained until it leaves through the lower boundary in axial direction. The topology is of type 0-0, which provides extremely good resolutions at trailing and leading edges as well as at the blade tip, compared with the total of cells needed. The main drawback is that the further the tip vortex convects past the blade, the greater the grid cells become, which is very disadvantageous since it causes vortex diffusion.

The second type of grid, having an H-topology, only covers the outer region of the rotor blade. This has the advantage that the grid fineness at the location where the tip vortex is captured, is similar to that one at the downstream boundary. The requirement of a lot of grid cells also at places where it is unefficient, can be compensated by covering only the most important part of the flow field region.

Calculations are presented for two two-bladed rotors under non-lifting as well as under hover conditions. One is full size with a realistic aspect ratio of 15 and the other one is a model rotor with an aspect ratio of 6. The collective pitch angles and tip Mach numbers are varied. The results of the second rotor are compared with the experimental data of Caradonna and Tung (Ref. 3).

2. Governing Equations

Due to the character of rotating flow, a blade-attached cylindrical coordinate system, rotating with the constant angular velocity $\vec{\omega}$ is chosen (Fig. 1).
Within this reference frame, the flow field of a hovering rotor can be treated as steady, but due to the rotation of the reference frame additional forces, the centrifugal and the Coriolis´ forces, have to be taken into account.
Thus the Euler equations can be written in differential conservation form:

$$\vec{\phi}_t + \frac{1}{r}\vec{E}_\varphi + \vec{F}_r + \vec{G}_z = \vec{K} \qquad (1)$$

with $\vec{\phi} = \begin{pmatrix} \rho \\ \rho u \\ \rho v \\ \rho w \\ e \end{pmatrix}$, $\vec{E} = \begin{pmatrix} \rho u \\ \rho u^2 + p \\ \rho uv \\ \rho uw \\ \rho uH \end{pmatrix}$, $\vec{F} = \begin{pmatrix} \rho v \\ \rho uv \\ \rho v^2 + p \\ \rho vw \\ \rho vH \end{pmatrix}$, $\vec{G} = \begin{pmatrix} \rho w \\ \rho uw \\ \rho vw \\ \rho w^2 + p \\ \rho wH \end{pmatrix}$

and $$\vec{K} = -\frac{\rho}{r}\begin{pmatrix} v \\ 2v\,(u-\Omega r) \\ (u-\Omega r)^2 - v^2 \\ vw \\ v(H-(\Omega r)^2) \end{pmatrix}$$

where $\vec{q} = \begin{pmatrix} u \\ v \\ w \end{pmatrix}$ is the vector of the relative velocity with respect to the blade-fixed coordinate system, with u being the circular, v the spanwise and w the vertical velocity component,

$\vec{\omega} = \begin{pmatrix} 0 \\ 0 \\ -\Omega \end{pmatrix}$ is the undisturbed angular flow velocity,

$\vec{\bar{q}} = \vec{q} - \vec{\omega} \times \vec{r} = \begin{pmatrix} \bar{u} \\ \bar{v} \\ \bar{w} \end{pmatrix} = \begin{pmatrix} u-\Omega r \\ v \\ w \end{pmatrix}$ is the vector of the disturbance velocity, which can also be called the absolute velocity,

$e = \frac{p}{\kappa-1} + \rho\frac{q^2}{2}$ is the total energy per unit volume,

$p = (\kappa-1)(e - \rho\frac{q^2}{2})$ is the static pressure,

and $H = \frac{e+p}{\rho}$ is the total enthalpy per unit mass.

Since a blade-fixed reference frame is used the usual transformation into curvilinar coordinates has to be done, which is described in detail in Ref. 2,6 and 8.
It was attempted to use the absolute instead of the relative velocities. Then the first momentum equation of Eq. (1) has to be replaced by:

$$(\rho\bar{u})_t + \frac{1}{r}(\rho u\bar{u} + p)_\varphi + (\rho\bar{u}\bar{v})_r + (\rho\bar{u}\bar{w})_z = -2\frac{\rho\overline{vu}}{r}$$

It was found that it doesn't make any significant difference, whether one uses the absolute or the relative velocities in the differential formulation of the Euler equations.

However, it is of decisive importance that all quantities used for extrapolation or interpolation within the numerical procedure do not contain any dependency on the freestream velocity $u_\infty = \Omega r$.
This fact concerns the velocity as well as the total energy. Details are described in section 4.

3. Grid Structures

The body-fitted grids used in the present paper are determined by an iterative solution of Poisson's equation, in which the source terms on the right-hand-side are evaluated by solving Laplace's equations (Ref.2). Thus we have three uncoupled fourth order equations for the three spatial directions:

$$\begin{aligned} X_{\xi\xi} + X_{\eta\eta} + X_{\zeta\zeta} &= P \\ Y_{\xi\xi} + Y_{\eta\eta} + Y_{\zeta\zeta} &= Q \\ Z_{\xi\xi} + Z_{\eta\eta} + Z_{\zeta\zeta} &= R \end{aligned}$$

$$\begin{aligned} P_{\xi\xi} + P_{\eta\eta} + P_{\zeta\zeta} &= 0 \\ Q_{\xi\xi} + Q_{\eta\eta} + Q_{\zeta\zeta} &= 0 \\ R_{\xi\xi} + R_{\eta\eta} + R_{\zeta\zeta} &= 0 \end{aligned}$$

In addition to this system, which provides to a high degree a very homogeneous distribution of grid lines, several mechanisms are envolved, used to manipulate this distribution in an advantageous way.
For example, it is possible to attract an arbitrary number of grid lines to the body's surface in order to have a finer resolution there, or to make the gridlines leave the surface under a specific angle.

According to the two various methods that are applied to discretizise the physical domain around the rotor blade(s), the grid topologies used are different.
In the first case the physical domain discretizised has the shape of a cylinder, containing the complete rotor disk as well as the helical wake (Type I). Due to symmetry effects, the use of only one cylinder half is sufficient when considering a two-bladed rotor in hover. This requires a periodical boundary condition for the flow values at the plane of symmetry (Fig. 2). The grid generated has an 0-0 topology, which provides a good resolution at the leading and trailing edge as well as at the tip region. Due to this advantages it is possible to have a relatively low total number of grid cells in spite of the large physical region to be covered and therefore, some "reserve" for grid refinement or grid embedding is left.
The results presented were obtained on a grid with a total of only 59 x 34 x 17 cells (59 cells around the profile, 34 on the blade surface in spanwise direction and 17 cells normal to the blade). The overall grid size for the full scale rotor is 20 chords in radial direction and the same from top to bottom, whereas an extension of 12 * 16 chords is chosen for the model rotor.
This rather coarse grid was originally planned to be used only for preliminary investigations to get principle informations how the Euler code works, but soon proved to provide relatively good global results as can be seen in section 5.
Nevertheless, in future work, the number of grid cells especially around and normal to the profile will be increased and some kind of grid refinement will be implemented in order to improve accuracy, in particular

concerning the convection of the tip vortex.

In the second case, intending to reduce the computational expense, not the complete rotor blade, but only its tip region is enclosed by the grid, starting at about 50-80 percent of the radius, depending on the blade's aspect ratio (Fig. 3a, Type IIa).
In order to have the ability to account for the influence of the tip vortex on the following blade, the boundaries up- and downstream of the blade are coplanar. For this reason an H-type topology has been chosen, which in addition has nearly the same spatial resolution along the expected tip vortex path, which is very advantageous as will be shown in this paper. The disadvantage of the H-grid is that it requires a greater total number of grid cells to achieve the same resolution in the blade's vicinity as an O-grid.

Fig. 3b shows another variation of the H-grid used, having a cuboidal instead of a bended shape (Type IIb).
In this case, the used cartesian coordinate system is not rotating but moves translatorically. The freestream velocity distribution is simulated by a shear flow and no additional forces appear. Beside this, the Euler code employed is nearly the same as that used for fixed wing applications. This proceeding is also used for instance by H. Stahl (Ref.12). The total of grid cells for the H-grids is 64 cells in streamwise, 25 cells in spanwise and 30 cells in normal direction. The overall size is 6 chords (respectively 7 for the model rotor) in radial and 9 chords in flow direction.

It is remarkable that for the global results of nearly the same quality, the total number of cells as a result of the H-structure is higher than for the O-O-grid, although the covered physical domain is considerably smaller.

4. Numerical Procedure

The Euler code used for the results presented is based on the EUFLEX code of A. Eberle of MBB. Details of this program are not specified in this paper, since they are described in an extensive manner in Ref. 1.
For a general overview only some basic features shall briefly be mentioned: The solution algorithm is a finite-volume method with the flow quantities refering to the cells' center. The time integration is performed as a one-step scheme, since for the present time only steady solutions are of interest, while the spatial differences are third or even higher order accurate. In order to have a hyperbolic system everywhere throughout the flowfield, the unsteady formulations of the Euler equations is chosen, even if only the steady solution is to be obtained.
The code is yet fully explicit providing a good degree of vectorization. Local time stepping as well as dimensional flux splitting is used. In order to avoid the disadvantages of other widely used Euler solvers, that need artificial viscosity terms to make the scheme stable and to prevent oscillations, the present code makes use of a method of asymmetric flux averaging onto the cell faces, that is based on the methods of characteristics and depends on the sign of the local eigenvalues.

To adjust this code to the requirements of the rotational flow of a hovering rotor, a lot of work had to be done in detail. However only one major feature shall be mentioned, since it has proved to be very essential: Due to the methods of characteristic flux averaging, the flux quantities on the cell faces are calculated by using interpolation or extrapolation schemes. These operations may only be done with quantities that are

independent of the freestream velocity $u_\infty = \Omega r$.
This concerns the circular component of the relative velocity $\vec{q}$ as well as the total energy e, which contains q^2.

Thus, two additional quantities have to be introduced:

$$\bar{u} = u - \Omega r \quad \text{(circular component of the absolute velocity)}$$

$$\bar{e} = e - \rho/2 \; \Omega r \; (2\bar{u} + \Omega r) \quad ,$$

which are used instead of u and e to carry out the characteristic flux averaging.
After doing this, the local value of Ωr at the exact physical location of the considered cell face is added to obtain the desired flux quantities. All the same the formulation of the Euler equations in terms of the relative flow values is retained, since this is more suitable for the solution algorithm derived from the method of characteristics.

In contrast to the original Euler code, in the present method the geometric mapping determinant has to be calculated, since the right-hand-side is not equal to zero. This is fulfilled by dividing the considered cell into five tetrahedra, whose volumes are determined by the method described in Ref. 9.

5. Results

The results that are presented in this paper were obtained for a full size rotor with an aspect ratio of 15 and for the model rotor of Caradonna and Tung (Ref. 3), that is commonly used by many authors to compare their results with reliable experimental data.
The blades are always untapered and untwisted and a NACA 0012 airfoil is used.
Fig. 4 shows the results of the full size rotor at a tip Mach number of 0.85. Since no experimental data are available, only a qualitative discussion of the results is possible.

The first row of Fig. 4 shows the isomachs and the pressure distribution for the hovering rotor at a collective pitch angle of 5^0. The pressure coefficient c_{pa} is related to the dynamic pressure at sonic speed. Beneath them the corresponding solutions for $\Theta_c = 0^0$ are plotted.
Both calculations were performed on the grid I (0-0 type, 59 x 34 x 17 cells), so that, by means of the periodical boundary condition, the blade vortex interaction could be taken into account for the hovering case. Details of the tip vortex propagation are described in the next section.

The two lower pairs of figures show the results of the calculations of the non-lifting case using the smaller grid II (H-type, 64 x 25 x 30 cells). Only the outer 20 percent of the rotor blade are embedded and a first order boundary condition is applied at the inner boundary, where the flow variables are extrapolated linear, except the spanwise velocity component v, instead of which q^2 is taken. It can be seen that the usage of the cuboidal grid (IIb) with a sheared freestream velocity profile provides nearly the same results as the bended grid (IIa).

A comparison with the solution obtained with the 0-0 grid also shows good agreement. Note that due to the different parts of the rotor blade covered by the meshes, different scale factors in spanwise direction are used for the plots.

In addition to the blade area itself, the character of the isomachs in the surrounding sphere is displayed in the lower figures, where the region of high velocity due to the effect of displacement can be seen to expand beyond the blade tip.

The subsequent calculations were done on the model rotor. Unlike the previous case, a quantitative comparison with experimental data at different radial sections is now possible (Fig. 5a + b).

For the first example, a tip Mach number of 0.815 and a collective pitch angle of 5 degrees is chosen.
The upper row of Fig. 5a shows the distribution of the pressure coefficient c_p which now, in contrast to c_{pa}, is refered to the dynamic pressure of the undisturbed flow at the respective local radial station. Taking into account that no boundary layer effects, which are of great influence especially in the nose and the shock region, can be considered by an inviscid method, the results show a very good agreement with the measurements, although no wake model at all is added. The influence of the blade vortex interaction was introduced only via the periodical boundary condition and is an implicit part of the Euler solution. Grid I was used for the calculations.

The great importance of the capability to involve the blade vortex interaction can be realized by drawing a compare to the curves in the lower row. In this case, an isolated rotor blade was investigated. The considerable deviations, i.e. the overprediction of the low-pressure distribution at the upper side and the underprediction on the lower side and herewith the overprediction of the local lift coefficient, could be assumed this way, since it is known, that the trailing wake of the advancing rotor blade decreases the effective angle of attack. The computations were done with the grid IIb as well as with grid I by replacing the periodical boundary condition, but only the results of grid IIb are shown since they are quite similar.

Two further combinations of tip Mach numbers and collective pitch angles are displayed in Fig. 5b, both being calculated with grid I.
The upper row contains the results of $M_{tip} = 0.439$ and $\Theta_c = 8^0$, while the lower row was obtained for $M_{tip} = 0.520$ and $\Theta_c = 0^0$.
Especially the first case was calculated by several authors, too (e.g. Ref. 4,11).
An interesting investigation was done by Roberts and Murman in Ref. 11, who inquired the variation of the results when employing more or less simplified stages of their wake model. A comparison shows that the quality of their results obtained with their full wake model is at least reached by the implicit method presented in this paper.

In the meantime, also a version of grid IIa has been generated for the application of periodical boundary conditions at the up- and downstream boundary. Its angle of aperture is 90 degrees, corresponding to a four-bladed rotor. The first results are expected in the near future.

One systematic deviation can be observed in the results obtained by grid I: In the nose region the value of the suction peak as well as the rate of pressure decrease are not predicted correctly. Both effects however can be diminished by increasing the number of mesh points in this region.

In the same manner as done in fig. 4, the results of the model rotor at $M_{tip} = 0.815$ and $\Theta_c = 5^0$ are qualitatively represented in fig. 6. The span- and chordwise variation of c_{pa} is shown. Again, the scale of the curves achieved with grid II is extended along the spanwise direction because the innermost spanwise station is located at about 48 percent of the blade radius. The boundary condition at this plane is the same linear extrapolation mentioned above.
The influence of the blade vortex interaction, already dealt with in fig. 5a,

can be seen more globally comparing the four top figures. The suction peak reaches a higher level and the low pressure regions show a greater extension in spanwise direction, whereas in chord direction the extensions do not differ.

Very good agreement is achieved between the calculations of the isolated rotor blade using grid I and grid IIb. The only differences are found in the shock region, where grid IIb provides a smaller shock. Reasons for this are not yet clear. In connection to that the typical overshooting behind the shock wave, often observed at inviscid procedures, does not appear in the results of grid I.

6. Tip Vortex Convection

One important question is, whether an Euler code is able to correctly predict effects depending on the trailing wake of the advancing rotor blade without any additional model.
Two main reasons are known to cause severe difficulties, the additional artificial viscosity terms involved in some solution algorithms on one hand and the truncation errors due to coarse grid regions on the other hand. Since the EUFLEX code makes no use of artificial viscosity terms, the first main problem is alleviated.
The alteration of the tip vortex structure when convecting along its path through partly very coarse grid regions is demonstrated in fig. 7. When viewing the figures, it must be considered, that for reasons of perceptibility the chosen scope as well as the scale factor for the velocity vectors had to be increased at a certain distance away from the blade. 45^0 and all the more 90^0 behind the blade, the vortex has diffused and has lost its intensity to a great amount, due to the fact, that the cell sizes increase rapidly.
However, when approaching the blade, the vortex regains its finer structure, and even the helical descendence of the core can be observed. Up to which degree the geometry of this vortex, when striking the blade, represents the physical truth is subject to further investigations.

The disadvantage of vortex diffusion due to grid coarseness is diminished when using the H-grid (Fig. 8).
Although the number of meshpoints within the frames reduces a little, the vortex diameter as well as the circular velocity components do not change significantly. Note that this time the framesize and the scale factor could be kept constant.

Fig. 9 shows the creation of the obviously weak inner vortex, that can only be captured, if an all enclosing grid is chosen.

7. Conclusions

The adjustment of a finite-volume Euler code, well proved for fixed wing applications, to helicopter flow fields has been presented. The Euler equations are formulated in terms of the relative flow variables with respect to a rotating blade-attached coordinate system.

The fundamental extension is the exclusive use of freestream independent flow variables within the numerical procedures when the characteristic flux averaging is performed.

For the way of discretizising the physical domain, two generally different philosophies have been applied, enclosing either the whole rotor disk or

only a segment of it around the blade tip region.

Results have been presented, providing very good agreements to experimental data. This fact shows the capability of the Euler solver to treat wake effects without needing any additional wake model.

However improvements have to be done concerning grid refinements in regions of high flow gradients and along the assumed vortex path.

References

1. Eberle, A. — A New Flux Extrapolation Scheme Solving the Euler Equations for Arbitrary 3-D Geometry and Speed, MBB-EUFLEX MBB/LKE122/S/PUB/140, 1984

2. Schwarz, W. — Dreidimensionale Netzgenerierung für ein Finites Volumenverfahren, MBB/LKE122/S/PUB/206, 1985

3. Caradonna, F.X.; Tung, C. — Experimental and Analytical Studies of a Model Helicopter Rotor in Hover, NASA TM-81232, 1981

4. Roberts, T.W.; Murman, E.M. — Solution Method for a Hovering Helicopter Rotor Using the Euler Equations, AIAA Paper 85-0436, 1985

5. Roberts, T.W.; Murman, E.M. — Euler Solutions for the Flow Around a Hovering Helicopter Rotor, AIAA Paper 86-1784, 1986

6. Sankar, N.L.; Wake, B.E.; Lekoudis, S.G. — Solution of the Unsteady Euler Equations for Fixed and Rotor Wing Configurations, AIAA Paper 85-0120, 1985

7. Sankar, N.L.; Tung, C. — Euler Calculations for Rotor Configurations in Unsteady Forward Flight, Proceedings of the 42nd Annual Meeting of the American Helicopter Society, Washington,D.C., 1986

8. Wake, B.E.; Sankar, N.L.; Lekoudis, S.G. — Computation of Rotor Blade Flows Using the Euler Equations, J. Aircraft, Vol. 23, No. 7, 1986, pp 582-588

9. Agarwal, R.K.; Deese, J.E. — Euler Calculations for Flowfield of a Helicopter Rotor in Hover, AIAA Paper 86-1782, 1986

10. Chang, I-Chung; Tung, C. — Euler Solution of the Transonic Flow for a Helicopter Rotor, AIAA Paper 87-0523, 1987

11. Kroll, N. — Computation of the Flow Fields of Propellers and Hovering Rotors Using Euler Equations, Proceedings of the 12th European Rotorcraft Forum, Garmisch-Partenkirchen, 1986

12. Stahl, H. — Application of a 3D Euler Code to Transonic Blade Tip Flow, Proceedings of the 12th European Rotorcraft Forum, Garmisch-Partenkirchen, 1986

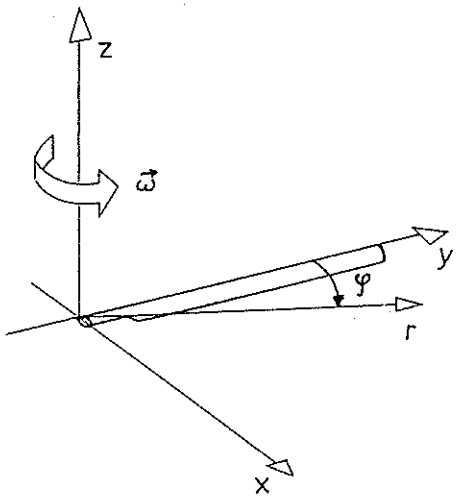

Fig.1: Blade-fitted coordinate system

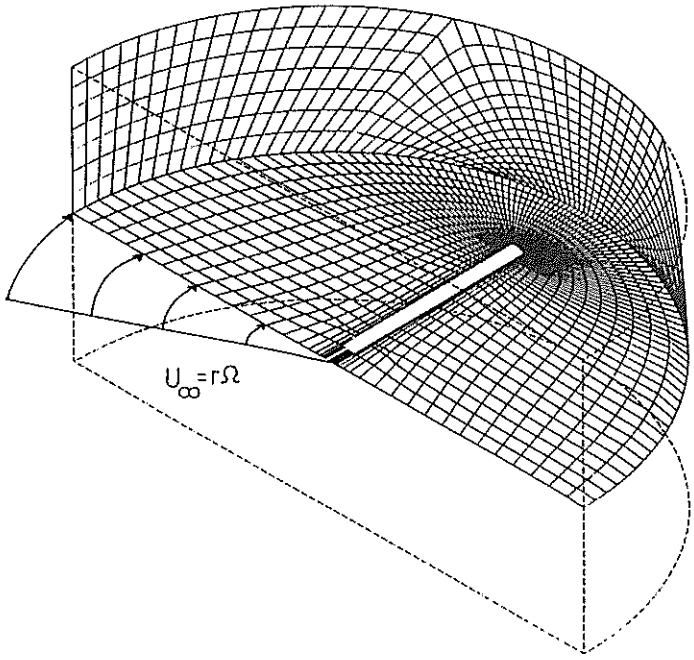

Fig.2: Grid type I: 0-0 topology, 59 x 34 x 17 cells
(Figure of the full size rotor with AR = 15)

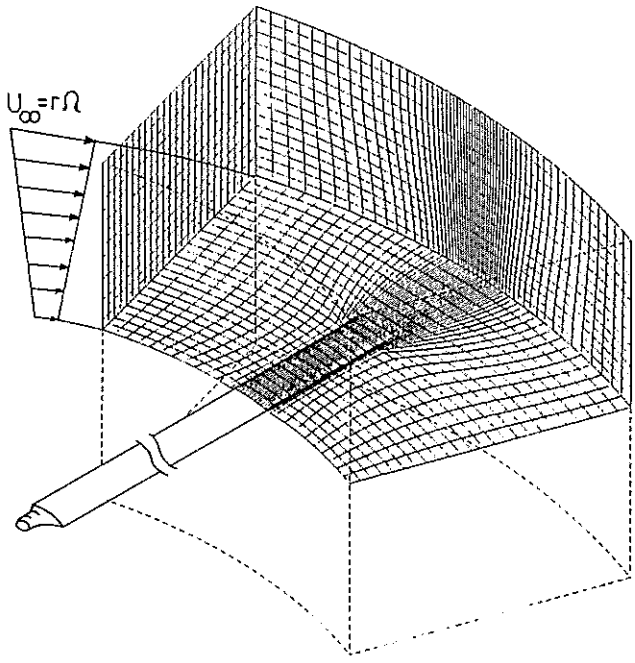

Fig.3a: Grid type IIa: H-topology, bended shape, 64 x 25 x 30 cells

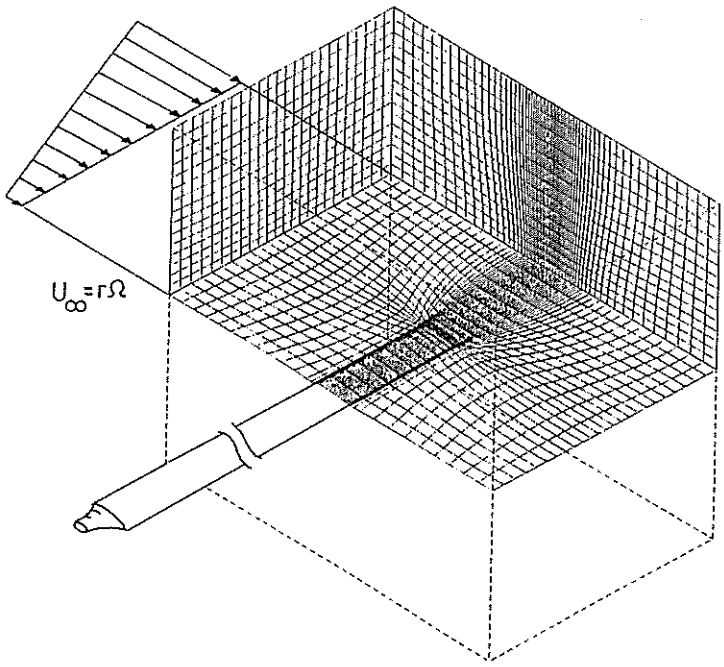

Fig.3b: Grid type IIb: H-topology, cuboidal shape, 64 x 25 x 30 cells

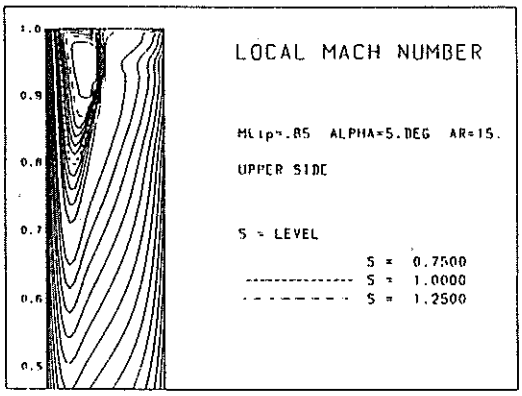

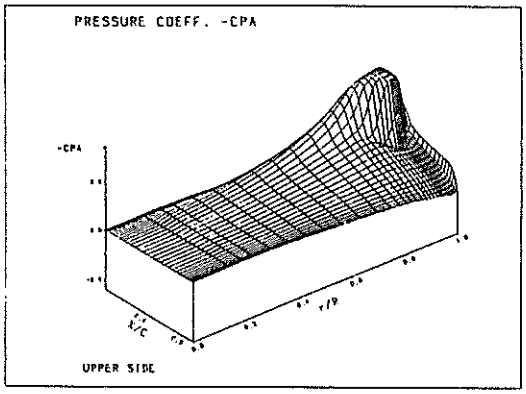

$\Theta_c = 5^0$, grid type I, blade vortex interaction considered

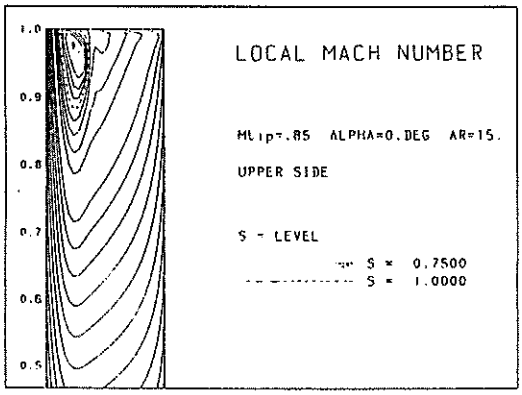

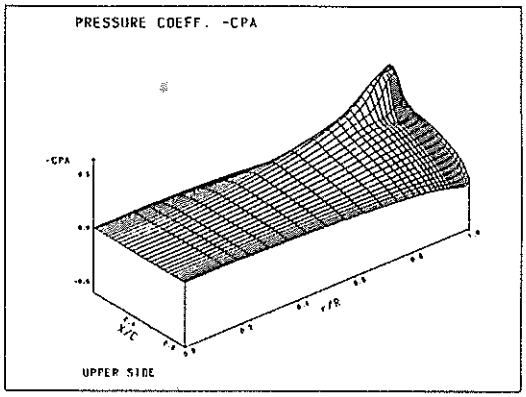

$\Theta_c = 0^0$, grid type I

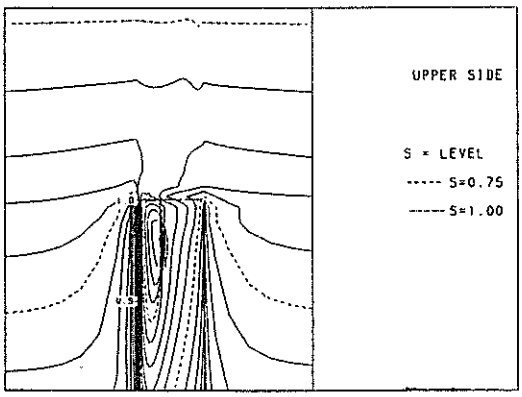

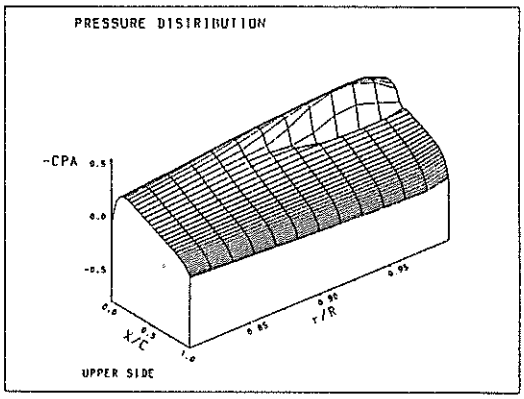

$\Theta_c = 0^0$, grid type IIa

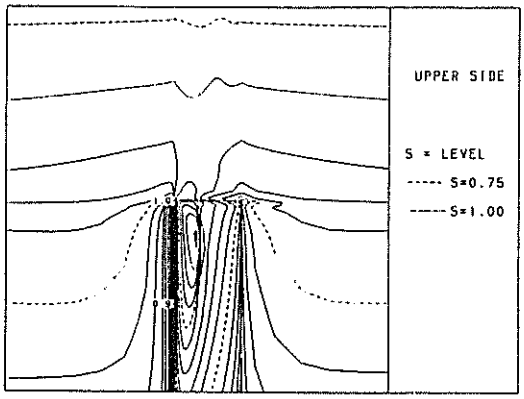

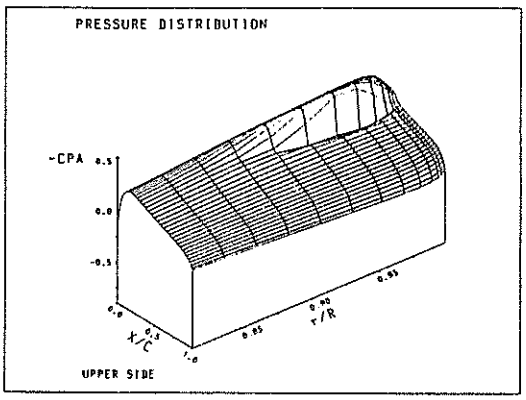

$\Theta_c = 0^0$, grid type IIb

Fig.4: Mach number and pressure distribution of a full size rotor with aspect ratio 15 and tip Mach number 0.85

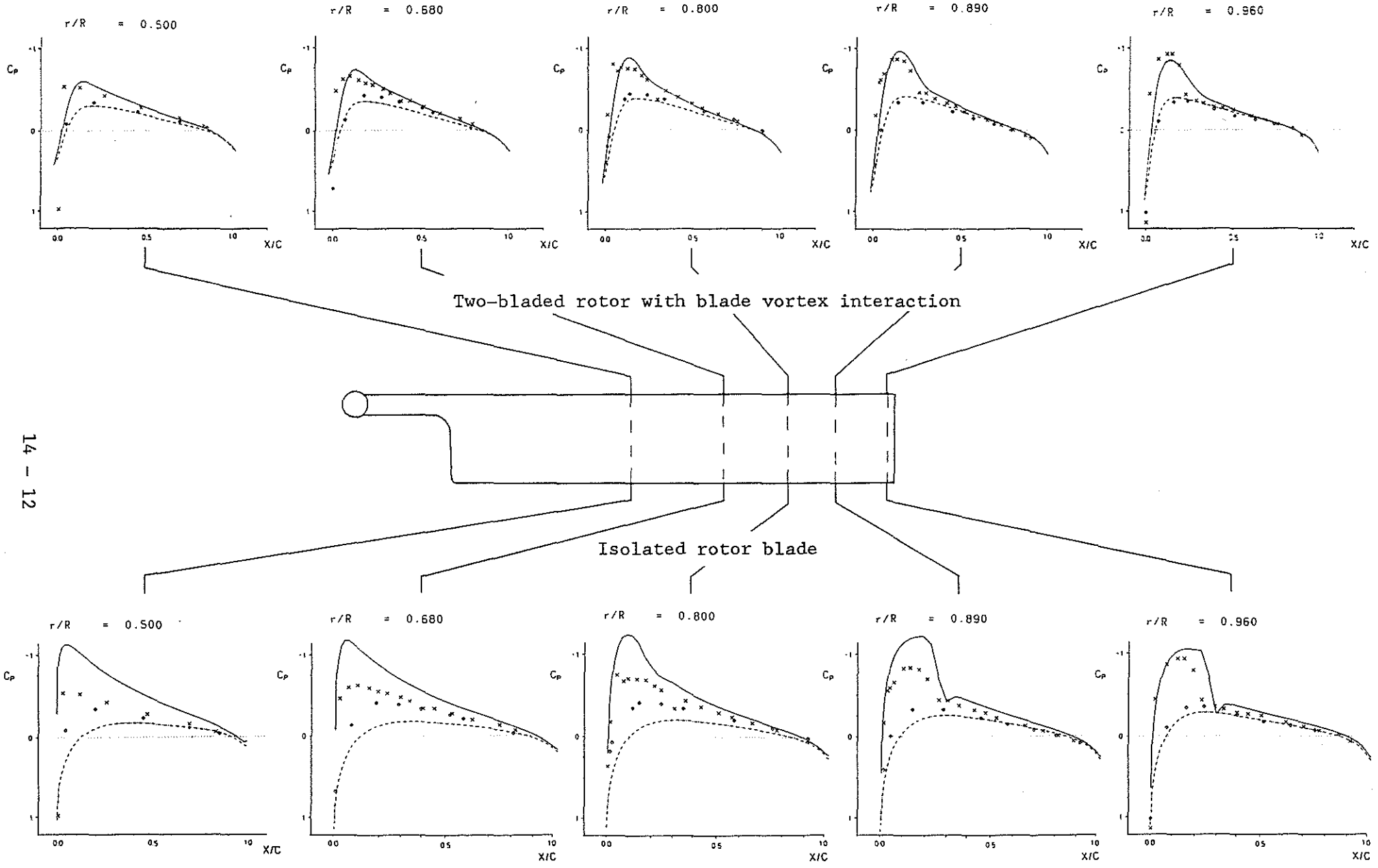

Fig.5a: Pressure distribution for the model rotor of Ref.3 (AR = 6, NACA 0012 airfoil), $M_{tip} = 0.815$, $\Theta_c = 5^0$. Comparison of calculations with (upper row) and without blade vortex interaction (lower row).

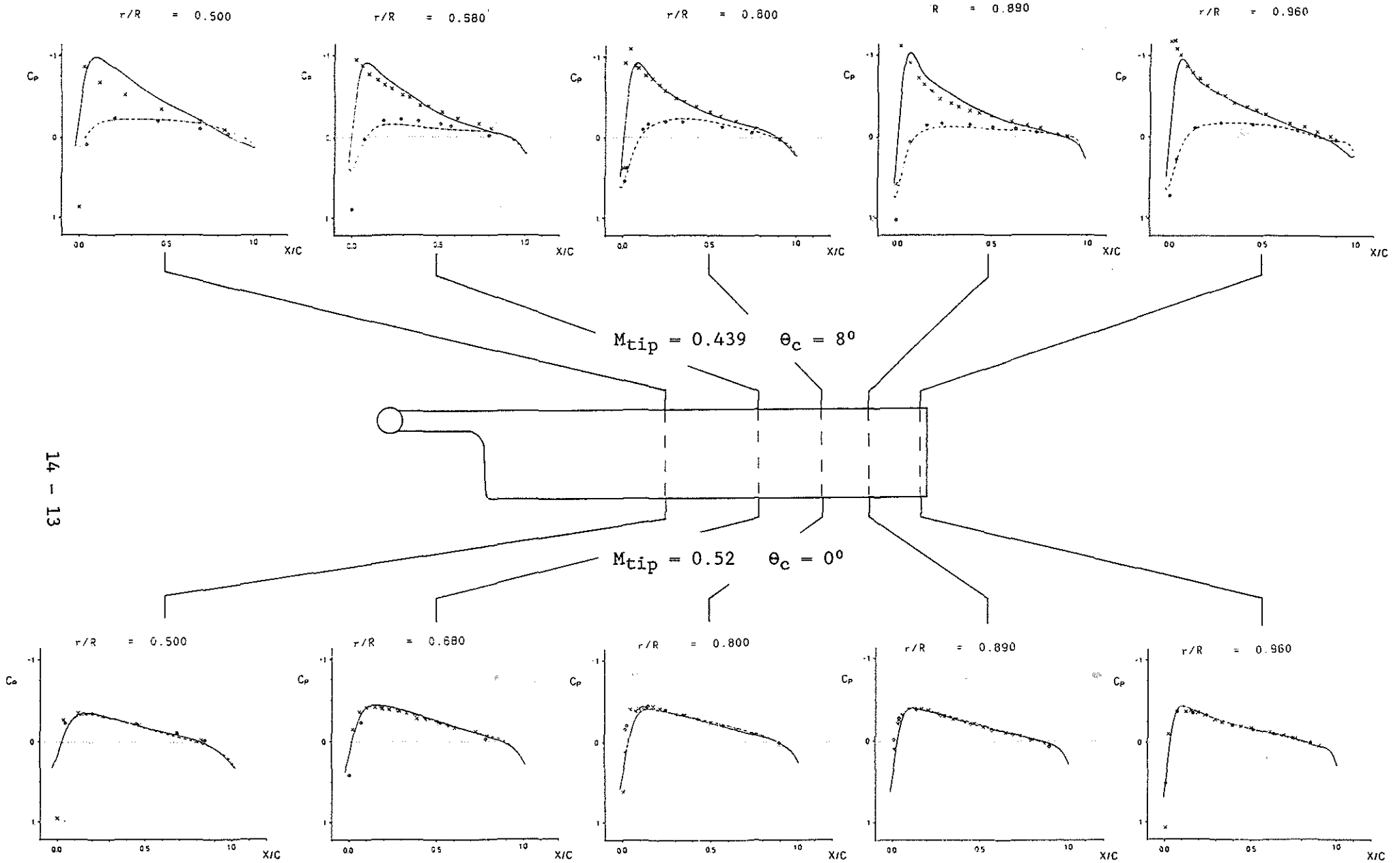

Fig.5b: Same model rotor at different tip Mach numbers and collective pitch angles. Hover case (lower row) calculated with blade vortex interaction. Comparison with experimental data of Ref. 3.

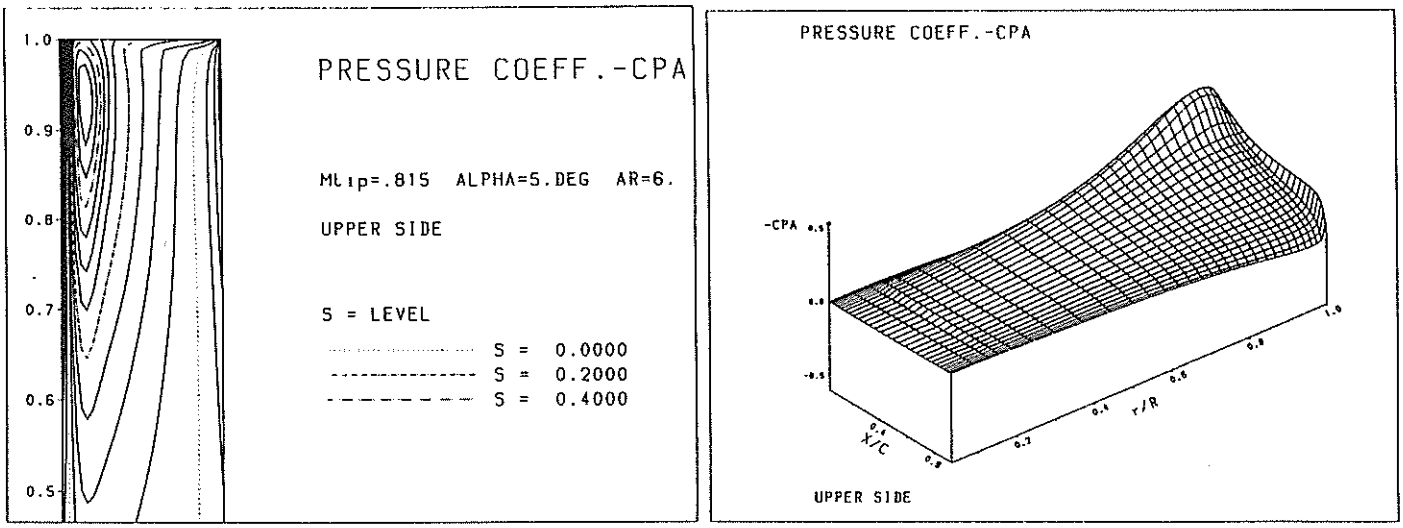

Blade vortex interaction considered, grid type I

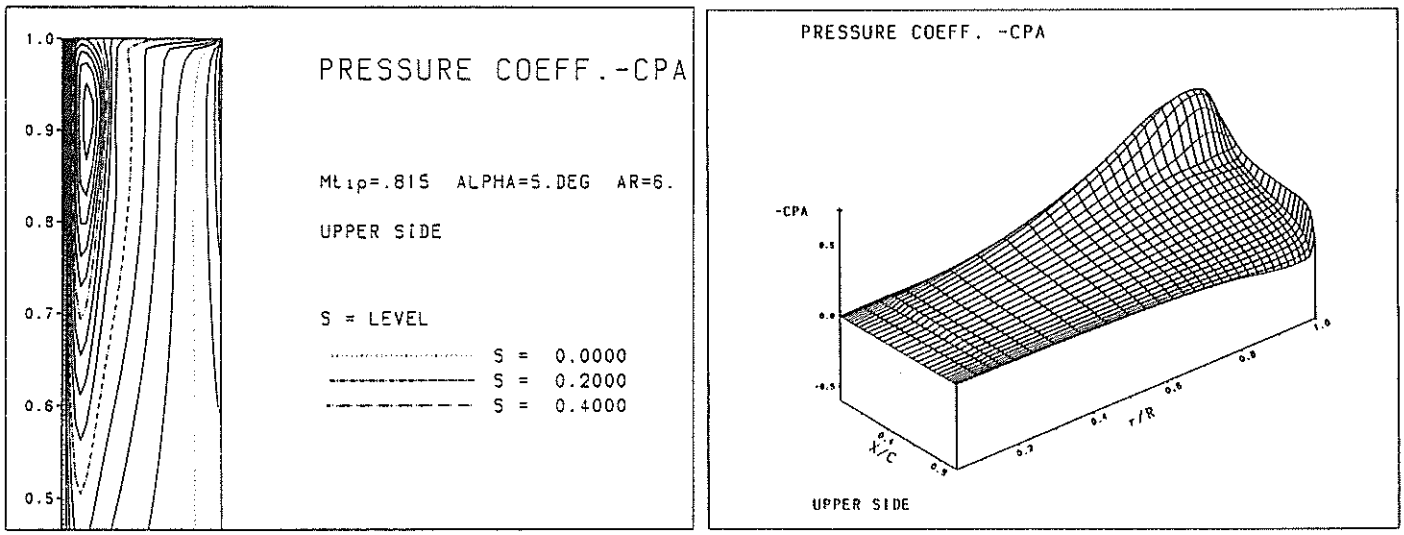

No blade vortex interaction, grid type I

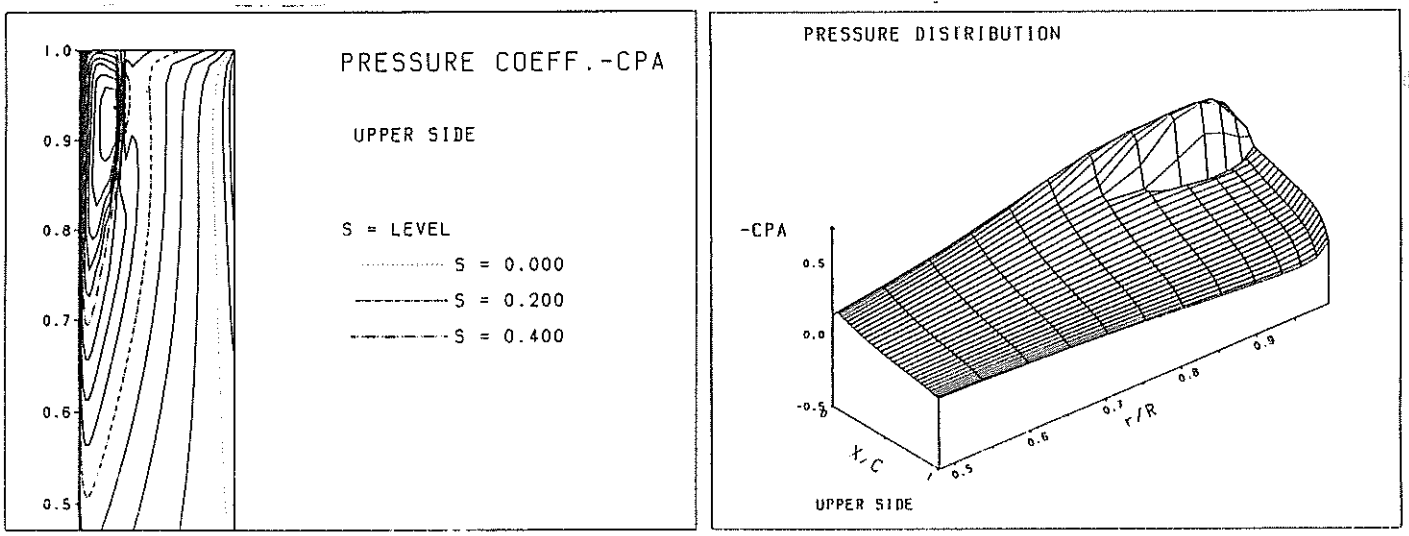

No blade vortex interaction, grid type IIb

Fig.6: Qualtitative representation of the surface pressure distribution and the isobars for the test case of Fig.5a (M_{tip} = 0.815, Θ_c = 5°).
Comparison of the results obtained with and without blade vortex interaction.

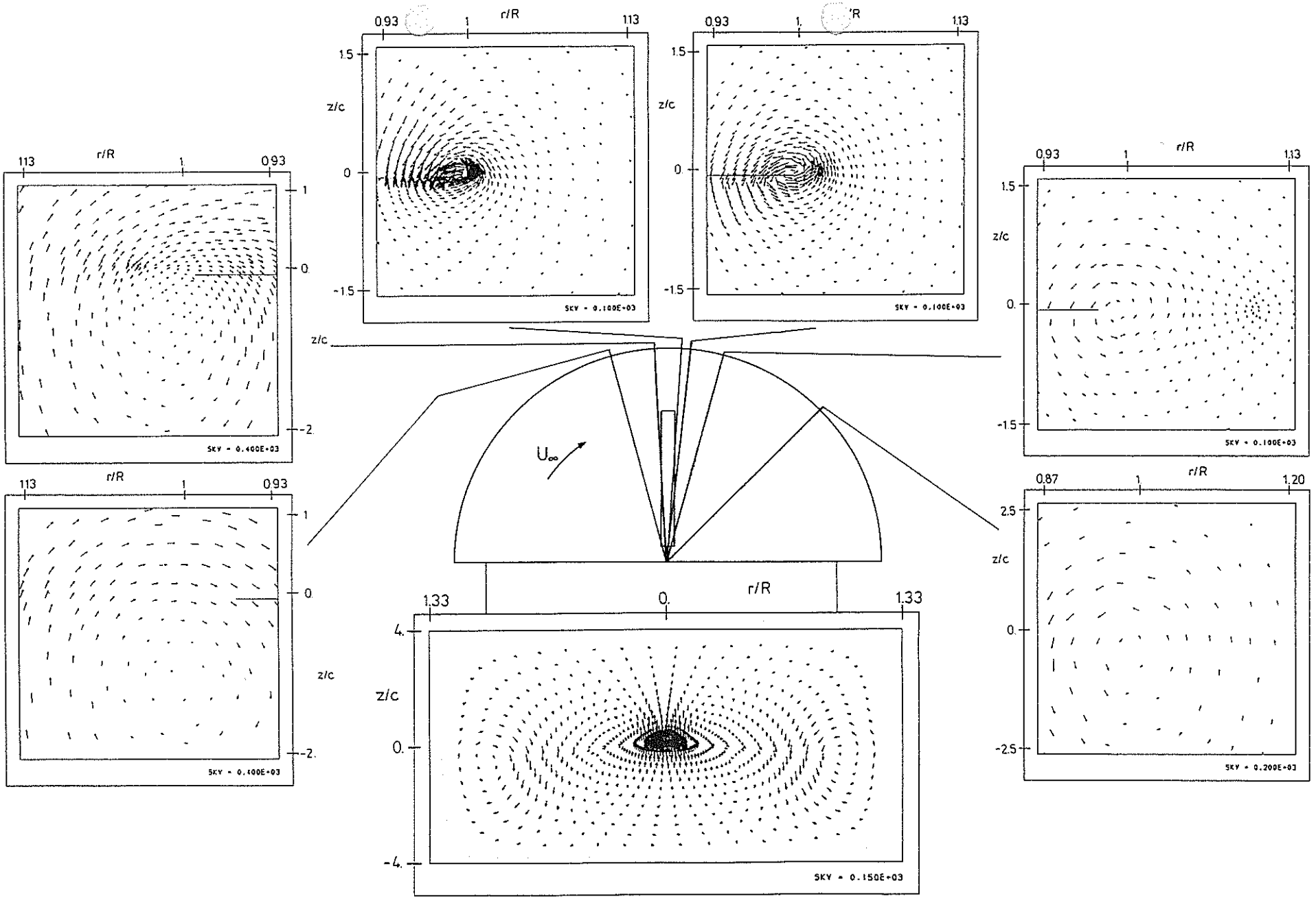

Fig.7: Tip vortex convection (grid type I, 59 x 34 x 17 cells)

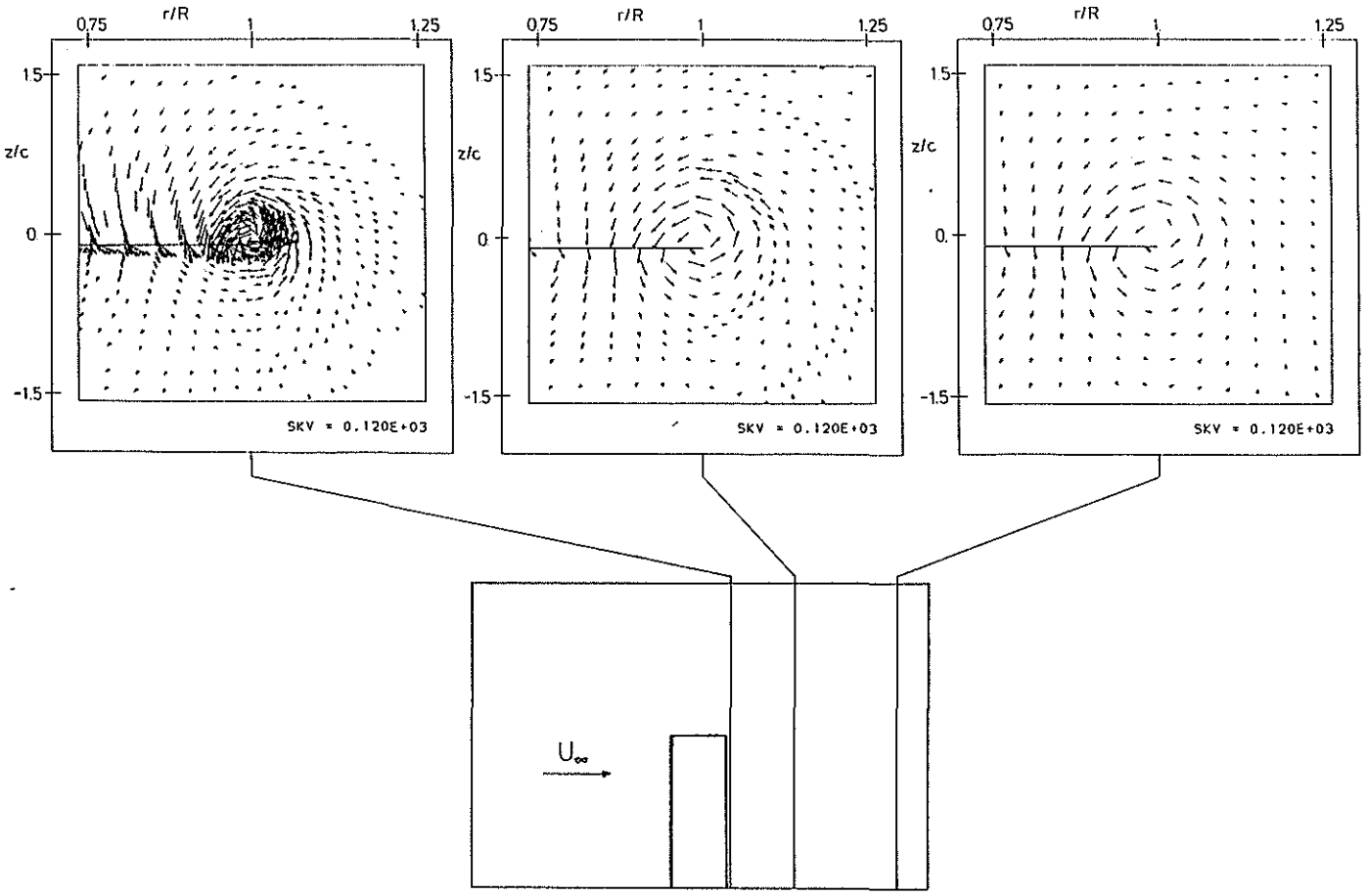

Fig.8: Tip vortex convection (grid type IIb, 64 x 25 x 30 cells)

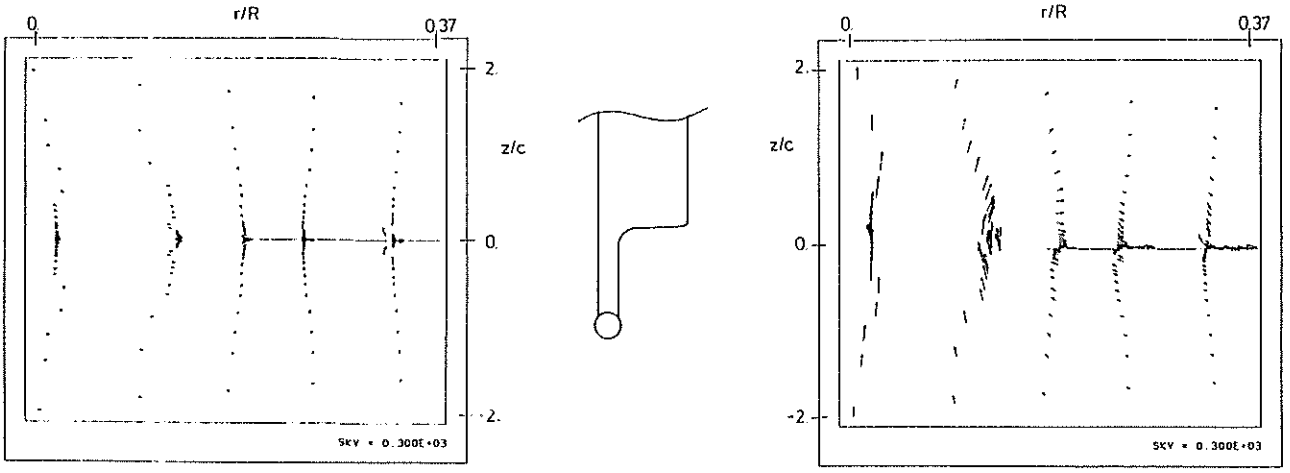

$\Theta_c = 0^0$ $\Theta_c = 5^0$

Fig.9: Inner vortex